Small interfering ribonucleic acid induces liquid-to-ripple phase transformation in a phospholipid membrane

Amit Choubey, Ken-ichi Nomura, Rajiv K. Kalia, Aiichiro Nakano, and Priya Vashishta

Collaboratory for Advanced Computing and Simulations, Department of Physics and Astronomy, Department of Computer Science, Department of Chemical Engineering and Materials Science, University of Southern California, Los Angeles, California 90089-0242, USA

Small interfering ribonucleic acid (siRNA) molecules play a pivotal role in silencing gene expression via the RNA interference mechanism. A key limitation to the widespread implementation of siRNA therapeutics is the difficulty of delivering siRNA-based drugs to cells. Here, we examine changes in the structure and dynamics of a dipalmitoylphosphatidylcholine bilayer in the presence of a siRNA molecule and mechanical barriers to siRNA transfection in the bilayer. Our all-atom molecular dynamics simulation shows that siRNA induces a liquid crystalline-to-ripple phase transformation in the bilayer. The ripple phase consists of a major region of non-interdigitated and a minor region of interdigitated lipid molecules with an intervening kink. In the ripple phase, hydrocarbon chains of lipid molecules have large compressive stresses, which present a considerable barrier to siRNA transfection. © 2014 AIP Publishing LLC. [http://dx.doi.org/10.1063/1.4896273]

Small interfering ribonucleic acid (siRNA) is a double-stranded molecule consisting of 21–25 nucleotides on each strand and 2 nucleotide overhangs at the $3'$ ends. It is well known that a bare siRNA molecule cannot easily cross a cell membrane because of its large molecular weight and negative charge on its backbone.[1] Since the discovery of RNA interference (RNAi), substantial effort has gone into developing strategies to deliver siRNA based drugs[1] that can directly destroy messenger RNA (mRNA) transcribed from oncogenes, potentially arresting pathological cell proliferation. RNAi also has the capacity to knock out other points in biochemical pathways, potentially crippling proliferative mechanisms at arbitrary "weak points." Strategies based on siRNA treatment have been investigated for gastric, colon, prostate, breast, lung, bladder, and ovarian cancer.[2]

Despite a great deal of experimental research, the effects of a bare siRNA on the structure and mechanics of a cell membrane are not well understood. Here, we examine molecular processes that give rise to siRNA-induced transfection barriers in a model biomembrane consisting of dipalmitoylphosphatidylcholine (DPPC) molecules at a temperature of 323 K and atmospheric pressure. Under these conditions, the thermodynamic state of a fully hydrated DPPC bilayer without the siRNA is the liquid crystalline phase L_α.[3–5] In this phase, DPPC molecules diffuse laterally and their hydrocarbon chains have conformational disorder in the form of *gauche* defects. Upon cooling at atmospheric pressure, the bilayer transforms into a ripple phase (labeled P_β) below a temperature of 315 K.[5] Upon further cooling, the DPPC bilayer first goes into a gel phase (labeled L_β) at $T = 308$ K and then crystallizes into a subgel or crystal phase at 280 K.[5] In the gel phase, hydrocarbon chains are nearly parallel and the membrane is thicker and less permeable than in the fluid phase. The characteristics of $L_\beta \rightarrow P_\beta$ and $P_\beta \rightarrow L_\alpha$ phase transformations have been studied both experimentally and by computer simulations.[6–25]

The structure of the ripple phase has been the subject of several experimental and theoretical investigations.[3,4,25]

X-ray studies indicate that the ripple phase in a DPPC bilayer consists of major (M) and minor (m) regions separated by kinks.[9–11] From X-ray data, the ripple length (λ_r), stacking repeat distance (d) and oblique angle (γ) have been extracted. Fourier transform infrared and ^{13}C-NMR measurements show a high degree of tail stretching of DPPC molecules in the ripple phase.[7,8] Differential scanning calorimetry,[26] X-ray[14] and neutron diffractions,[9] scanning-tunneling microscopy,[13] and freeze-fracture electron microscopy[9,14] have also been used to study the ripple phase. Experiments indicate that the size of the hydrated head group, the tilt of acyl chains, the extent of the chain movement, and the strength of intraleaflet interactions are the key determinants of the ripple phase.[14] Sengupta *et al.*[10] have used electron density maps to establish that the average chain tilt along the direction of rippling is responsible for ripples. Other models assume that ripples form to relieve packing frustrations when the relationship between the cross-sectional areas of head groups and apolar tails exceeds a certain threshold.[15] It has also been suggested that periodic local spontaneous curvature in lipid bilayers gives rise to ripples. The local spontaneous curvature could arise from electrostatic coupling between water molecules and polar lipid head groups, coupling between membrane curvature and molecular tilt, or the generation of curvature by linear arrays of fluid state lipid molecules.[15]

Several simulation studies have also reported the formation of ripple phases. Lenz and Schmid[20] used Monte Carlo simulations of a coarse-grained molecular model for lipid-solvent mixtures to study ripple phases. They find that the head group and tail size mismatch and interdigitation were important factors in the ripple-phase formation. Mesoscopic simulations by Kranenburg *et al.*[23] indicate that the frustration arising from the surface area of head groups and the lateral density of lipid tails is a key factor in the formation of ripple phases.

In this paper, we present an all-atom molecular dynamics (MD) simulation study of a DPPC bilayer interacting with a

bare siRNA molecule. Figure 1 is a snapshot of the simulated system comprising a siRNA, 648 DPPC, and 216 100 water molecules, and 40 sodium ions to maintain charge neutrality in the system.[27,28] In our simulations, the siRNA sequence is ss(UU)-ds(GACAGCAUAUAUGCUGUC)-ss(UU). The MD cell contained 733 917 atoms and the initial dimensions of the cell were $14.4 \times 14.4 \times 38.6$ nm^3. The pre-equilibrated DPPC membrane was taken from Ref. 29 and replicated in the x and y directions to generate a membrane of cross-sectional area 14.4×14.4 nm^2. The MD simulation was carried out with CHARMM 36 force field[30–32] using the GROMACS MD package.[33] Periodic boundary conditions were imposed, and the particle mesh Ewald method was used to compute the long-range Coulomb interaction.[34] The real-space contributions to Coulomb potential and forces were calculated with a cutoff of 1.0 nm, and the Fourier-space contributions were calculated on a mesh of 0.15 nm. The non-bonded Lennard-Jones interaction was calculated with a cut-off of 1.2 nm. The simulation was carried out in the isothermal-isobaric ensemble using a Nosé-Hoover thermostat[35] to maintain the temperature at 323 K and Parrinello-Rahman barostat to keep the pressure at 1 bar.[36] Interatomic bond lengths were constrained using the LINCS algorithm.[37] Equations of motion were integrated with the velocity-Verlet algorithm using a time step of 1 fs and the simulation was run for 500 ns.

The siRNA induces significant changes in the structure of the DPPC bilayer. Figure 2 gives an overall view of the membrane structure at time $t = 500$ ns. In Fig. 2(a), the head groups and tails of lipid molecules in the distal leaflet (farther from the siRNA) are blue and cyan, respectively, and lipid tails of the proximal leaflet are brown. The patchiness in the x-y plane of the membrane indicates significant variation in the membrane thickness. To quantify this, we divided the membrane into 200×200 pixels in the x-y plane and calculated the bilayer thickness in each pixel[38] (The bilayer thickness, D, in a pixel is defined as the maximum distance between the lipid head groups in the proximal and distal leaflets.) Figure 2(b) shows the distribution functions for membrane thickness at time $t = 2$ ns and 500 ns. At 2 ns the distribution function has a single peak,
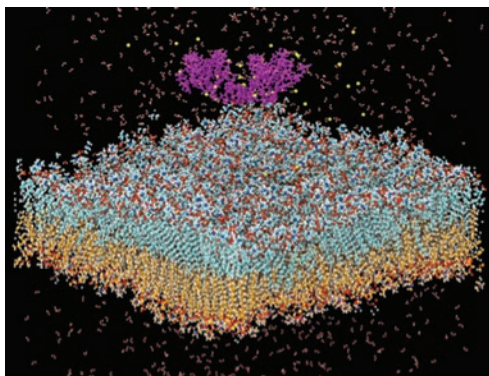

FIG. 1. A snapshot of the system at time $t = 10$ ns. The siRNA is shown in magenta, sodium ions are yellow, and carbon tails of proximal and distal leaflets of the DPPC bilayer are cyan and orange spheres, respectively. Blue and red spheres represent lipid head groups. Only a few water molecules (red and white dots) are shown here.
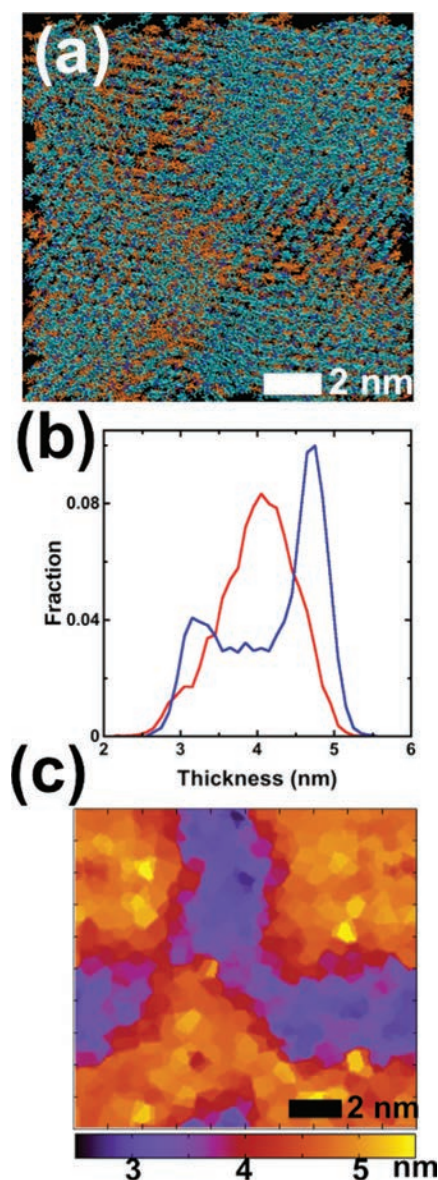

FIG. 2. (a) Top view of the lipid bilayer from the distal side of the siRNA. The head groups and tails of lipid molecules in the distal leaflet are blue and cyan, respectively, and the lipid tails of the proximal leaflet are brown. (b) Bilayer-thickness distributions for the fluid phase at time $t = 2$ ns (in red) and the ripple phase at $t = 500$ ns (in blue). The distribution at 2 ns is similar to distribution obtained from another 50 ns MD simulation of DPPC bilayer without siRNA. (c) Pixelated membrane thickness shows the major (orange and red) and minor (purple) regions of the ripple phase.

indicating that the membrane is uniform and its thickness is about 3.7 nm. As time evolves, the membrane thickness develops a bi-modal distribution and at $t = 500$ ns, the distribution function has a prominent peak around 4.7 nm and a smaller one around 3.0 nm. Figure 2(c) is a color-coded snapshot of the membrane thickness in 200×200 pixels at $t = 500$ ns. Here, the membrane thicknesses in the major (orange) and minor (purple) regions are $D_M \approx 4.7$ nm and $D_m \approx 3.0$ nm, respectively.

In Fig. 3, panels (a) and (b) present side views of the bilayer structure in minor and major regions, respectively, at time $t = 500$ ns. Here, the lipid head groups and hydrocarbon tails in the proximal leaflet of the DPPC bilayer are blue and
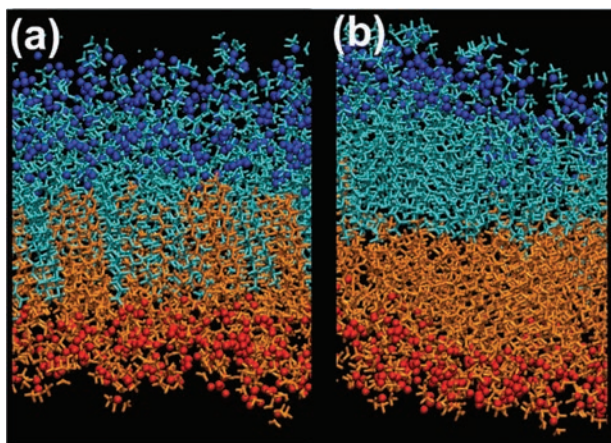
FIG. 3. Cross-sectional snapshot of the DPPC bilayer at time $t = 500$ ns shows interdigitated (a) and non-interdigitated (b) lipid molecules in the siRNA-induced ripple phase. In the top leaflet, the head groups and lipid tails are blue and cyan, and in the bottom leaflet, they are red and orange, respectively.

FIG. 5. Lateral stress profile normal to the lipid membrane (z-direction). Compressive stresses in lipid tails between -1.5 nm and 1.5 nm are enhanced by the presence of siRNA.

cyan, and in the distal leaflet, they are red and brown, respectively. Figures 3(a) and 3(b) show that the minor region consists of interdigitated and the major region contains non-interdigitated lipid molecules. These snapshots also show that lipid molecules in major and minor regions are tilted relative to the bilayer normal, i.e., the z-axis. The average tilt angle θ is around $26°$ for the patch of noninterdigitated lipid molecules. The experimental value of θ in the gel phase of a fully hydrated DPPC bilayer is $32°$.[39] It should be noted that the siRNA molecule is freely diffusing and we find no correlations between the lateral location of the siRNA and any specific region of the bilayer.

The major and minor regions make up almost entirely the ripple phase of the DPPC bilayer. Figure 4 is a snapshot of the ripple phase taken at $t = 500$ ns. We have used such snapshots to estimate the average wavelength (λ_r), amplitude (A), tilt angle (γ), and widths of the major (d_M) and minor (d_m) regions. We find $\lambda_r = 10.85$ nm, $A = 1.07$ nm, $\gamma = 104°$, $d_M = 3.33$ nm, and $d_m = 1.41$ nm. Freeze-fracture electron microscopy and X-ray diffraction studies indicate that $\lambda_r \sim 13$ nm and $\gamma = 95°$ for the ripple structure in DPPC and that the hydrocarbon chains in the ripple phase are tilted relative to the normal to the bilayer plane.

de Vries *et al.* have performed all-atom MD simulations to study the ripple-phase structure in lecithin bilayers.[25] They observe that the interdigitated patch connects the neighboring noninterdigitated region such that the upper leaflet of the bilayer on one side crosses over into the lower leaflet on the other side. They find that $\lambda_r = 12–16$ nm,
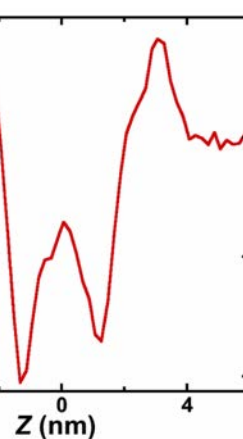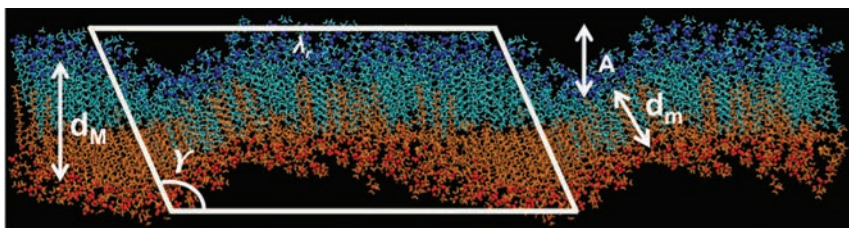
$A = 2.4$ nm, $\gamma = 56°–118°$, $d_M = 4.6$ nm, and $d_m = 3.2$ nm for the ripple phase in the DPPC membrane.

In our simulation, we notice that hydrocarbon tails of lipid molecules in major and minor regions are almost straight whereas in the intervening kink they are disordered. To quantify this disorder in kinks, we calculated gauche defect distribution function in lipid tails and found peaks around $\pm68°$. These peaks are similar to the peaks in the distribution function for gauche defects in the L_α phase. Furthermore, the planar (x-y) self-diffusion coefficient of lipid molecules in the kink region has nearly the same value as in the L_α phase. Together, the gauche defect density and lipid diffusion indicate that the kink region is akin to the L_α phase of the DPPC bilayer.

In the major and minor regions of the ripple phase, lipids are more closely packed and stresses in hydrophobic tails are more compressive than in the L_α phase. To quantify this, we calculated the stress tensor (see also the supplementary material[40])[41]

$$\overset{\leftrightarrow}{P} = \sum_i m_i \vec{v}_i \otimes \vec{v}_i + \frac{1}{V} \sum_{i<j} \vec{r}_{ij} \otimes \vec{F}_{ij}, \quad (1)$$

where m_i is the mass of the ith atom, $\vec{v}_i$ is its velocity, and $\vec{r}_{ij}$ and $\vec{F}_{ij}$ are the position vector and force between atoms i and j, respectively. Figure 5 shows the stress $\pi(z) = (P_{xx} + P_{yy})/2 - P_{zz}$ as a function of the distance z normal to the bilayer plane in the ripple phase (see also Figs. S1 and S2 in the supplementary material[40]). Here, positive peaks indicate membrane expansion in the lipid head-group region, and negative peaks imply membrane compression in lipid tails. Evidently, the siRNA reduces the positive lateral pressure in the head-

FIG. 4. Ripple phase is shown with the ripple vector in the horizontal direction at $t = 500$ ns. The ripple phase parameters are $\lambda_r = 10.85$ nm, $A = 1.07$ nm, $\gamma = 104°$, $d_M = 3.33$ nm, and $d_m = 1.41$ nm.

group region while enhancing the compressive stress significantly in lipid tails.

In summary, our all-atom MD simulation shows that the siRNA induces a liquid crystalline-to-ripple phase transformation in the bilayer. The ripple phase consists of a major region of non-interdigitated and a minor region of interdigitated lipid molecules with an intervening kink. The bilayer thicknesses in the major and minor regions are 4.7 nm and 3.0 nm, respectively. There is experimental evidence for interdigitation of lipid molecules in the presence of anions: Lesslaue *et al.*[42] report that the anionic fluorescent probe 1-anilino-8-naphthalene sulfonate decreases the lipid bilayer thickness to 3 nm because of interdigitation of lipid chains. X-ray diffraction data show that chlorpromazine also reduces the bilayer thickness from 5 nm to 3 nm.[43] In the ripple phase, we find large compressive stresses in lipid tails, which present a considerable barrier to siRNA transfection across the bilayer. To facilitate siRNA transfection, it is essential to lower the mechanical barrier arising from large compressive stresses in the ripple phase. Experiments indicate that cationic nanoparticles fluidize the gel phase of lipid vesicles,[44] and encapsulation in cationic liposomes enhances the transfection efficiency of siRNA molecules.[2]

[1] A. Fire, S. Q. Xu, M. K. Montgomery, S. A. Kostas, S. E. Driver, and C. C. Mello, Nature **391**(6669), 806–811 (1998).

[2] K. A. Whitehead, R. Langer, and D. G. Anderson, Nat. Rev. Drug Discovery **8**(6), 516 (2009).

[3] W. J. Sun, S. Tristram-Nagle, R. M. Suter, and J. F. Nagle, Proc. Natl. Acad. Sci. U.S.A. **93**(14), 7008–7012 (1996).

[4] M. Rappolt, G. Pabst, G. Rapp, M. Kriechbaum, H. Amenitsch, C. Krenn, S. Bernstorff, and P. Laggner, Eur. Biophys. J. Biophys. Lett. **29**(2), 125–133 (2000).

[5] S. Tristram-Nagle and J. F. Nagle, Chem. Phys. Lipids **127**(1), 3–14 (2004).

[6] X. Y. Wang, K. Semmler, W. Richter, and P. J. Quinn, Arch. Biochem. Biophys. **377**(2), 304–314 (2000).

[7] D. G. Cameron, H. L. Casal, and H. H. Mantsch, Biochemistry **19**(16), 3665–3672 (1980).

[8] R. J. Wittebort, C. F. Schmidt, and R. G. Griffin, Biochemistry **20**(14), 4223–4228 (1981).

[9] B. A. Cunningham, A.-D. Brown, D. H. Wolfe, W. P. Williams, and A. Brain, Phys. Rev. E **58**(3), 3662–3672 (1998).

[10] K. Sengupta, V. A. Raghunathan, and J. Katsaras, Europhys. Lett. **49**(6), 722–728 (2000).

[11] H. Yao, S. Matuoka, B. Tenchov, and I. Hatta, Biophys. J. **59**(1), 252–255 (1991).

[12] D. V. Soloviov, Y. E. Gorshkova, O. I. Ivankov, A. N. Zhigunov, L. A. Bulavin, V. I. Gordeliy, and A. I. Kuklin, J. Phys. Conf. Ser. **351**, 012010 (2012).

[13] J. T. Woodward and J. A. Zasadzinski, Biophys. J. **72**(2), 964–976 (1997).

[14] D. M. Czajkowsky, C. Huang, and Z. F. Shao, Biochemistry **34**(39), 12501–12505 (1995).

[15] T. Kaasgaard, C. Leidy, J. H. Crowe, O. G. Mouritsen, and K. Jorgensen, Biophys. J. **85**(1), 350–360 (2003).

[16] Z. V. Leonenko, E. Finot, H. Ma, T. E. Dahms, and D. T. Cramb, Biophys. J. **86**(6), 3783–3793 (2004).

[17] C. Cametti, F. Deluca, A. Dilario, M. A. Macri, G. Briganti, and B. Maraviglia, Prog. Colloid Polym. Sci. **84**, 465–469 (1991).

[18] K. Honda and H. Kimura, J. Phys. Soc. Jpn. **60**(4), 1212–1215 (1991).

[19] M. L. Belaya, M. V. Feigelman, and V. G. Levadny, J. Phys. II France **1**(3), 375–380 (1991).

[20] O. Lenz and F. Schmid, Phys. Rev. Lett. **98**(5), 058104 (2007).

[21] W. S. McCullough and H. L. Scott, Biophys. J. **57**(2), A473 (1990).

[22] P. A. Pearce and H. L. Scott, J. Chem. Phys. **77**(2), 951–958 (1982).

[23] M. Kranenburg, C. Laforge, and B. Smit, Phys. Chem. Chem. Phys. **6**(19), 4531–4534 (2004).

[24] M. A. Kamal, A. Pal, V. A. Raghunathan, and M. Rao, Europhys. Lett. **95**(4), 48004 (2011).

[25] A. H. de Vries, S. Yefimov, A. E. Mark, and S. J. Marrink, Proc. Natl. Acad. Sci. U.S.A. **102**(15), 5392–5396 (2005).

[26] R. N. A. H. Lewis, N. Mak, and R. N. Mcelhaney, Biochemistry **26**(19), 6118–6126 (1987).

[27] P. K. Maiti, T. A. Pascal, N. Vaidehi, J. Heo, and W. A. Goddard, Biophys. J. **90**(5), 1463–1479 (2006).

[28] S. A. Pandit and M. L. Berkowitz, Biophys. J. **82**(4), 1818–1827 (2002).

[29] J. B. Klauda, R. M. Venable, J. A. Freites, J. W. O'Connor, C. Mondragon-Ramirez, I. Vorobyov, D. J. Tobias, A. D. MacKerell, and R. W. Pastor, J. Phys. Chem. B **114**, 7830–7843 (2010).

[30] P. Bjelkmar, P. Larsson, M. A. Cuendet, B. Hess, and E. Lindahl, J. Chem. Theory Comput. **6**(2), 459–466 (2010).

[31] S. E. Feller and A. D. MacKerell, J. Phys. Chem. B **104**(31), 7510–7515 (2000).

[32] A. D. MacKerell and N. K. Banavali, J. Comput. Chem. **21**(2), 105–120 (2000).

[33] B. Hess, C. Kutzner, D. van der Spoel, and E. Lindahl, J. Chem. Theory Comput. **4**(3), 435–447 (2008).

[34] U. Essmann, L. Perera, M. L. Berkowitz, T. Darden, H. Lee, and L. G. Pedersen, J. Chem. Phys. **103**(19), 8577–8593 (1995).

[35] W. G. Hoover, Phys. Rev. A **31**(3), 1695–1697 (1985).

[36] S. Nose and M. L. Klein, Mol. Phys. **50**(5), 1055–1076 (1983).

[37] B. Hess, H. Bekker, H. J. C. Berendsen, and J. G. E. M. Fraaije, J. Comput. Chem. **18**(12), 1463–1472 (1997).

[38] W. J. Allen, J. A. Lemkul, and D. R. Bevan, J. Comput. Chem. **30**(12), 1952–1958 (2009).

[39] J. F. Nagle and S. Tristram-Nagle, Biochim. Biophys. Acta Rev. Biomembr. **1469**(3), 159–195 (2000).

[40] See supplementary material at http://dx.doi.org/10.1063/1.4896273 for simulation details.

[41] O. H. S. Ollila, H. J. Risselada, M. Louhivuori, E. Lindahl, I. Vattulainen, and S. J. Marrink, Phys. Rev. Lett. **102**(7), 078101 (2009).

[42] W. Lesslaue, J. E. Cain, and J. K. Blasie, Proc. Natl. Acad. Sci. U.S.A. **69**(6), 1499 (1972).

[43] T. J. Mcintosh, R. V. Mcdaniel, and S. A. Simon, Biochim. Biophys. Acta. **731**(1), 109–114 (1983).

[44] B. Wang, L. F. Zhang, S. C. Bae, and S. Granick, Proc. Natl. Acad. Sci. U.S.A. **105**(47), 18171–18175 (2008).